Experimental Validation of a Novel Wind Turbine Blade Power Optimization Methodology for Skewed Fluid Flow

Emelia K. Clark*, Matthew S. Simpson †, Trevor L. Joncich ‡, Saurabh Agrawal §
North Carolina State University, Raleigh, NC 27695

Designing wind turbine blade profiles to maximize fluid energy harvest is imperative for the cost optimization of renewable wind energy technology. The theoretical maximum kinetic energy harvesting for turbines is defined by Betz's limit. Software like QBlade, which is based on blade element momentum theory, can be used to analyze turbines for efficiency determination. This software contains tools for Betz optimization in axial flow conditions, but real-world wind profiles are rarely axial to the turbine, leading to the majority of flow entering the turbine being skewed relative to the turbine. To optimize turbine operation in skewed flow, an airfoil optimization script was written in MATLAB, using a genetic algorithm for maximization of lift over drag of each elemental blade section. With input design parameters of inflow velocity magnitude, skew angle and a 0.15 meter blade radius, a study was conducted for blades at 20 and 30 degrees of skew with 5 meters per second inflow velocity. The chord parameters of each blade segment were then determined utilizing optimal rotor theory, and twist was optimized using a novel methodology to maximize the power coefficient specifically. To validate this optimization schema, QBLADE was utilized to perform the blade element momentum theory analysis required for the determination of the power output of the multi-blade turbine, and the native Betz twist optimization tool was run with the inflow velocity with skew for comparison. To validate the theoretical results, each blade was utilized in a subsonic wind tunnel environment at different skew angles and different fluid flow speeds. Rotor angular rate, 3-axis force measurement, and power generated were all measured as a function of flow speed. The results of the experiment were compared with both theoretical results, and it was observed that the novel twist optimization methodology yielded higher power coefficients at optimal skew conditions.

I. Nomenclature

A	=	blade swept area
a	=	axial induction factor
a'	=	tangential induction factor
α	=	angle of attack
β	=	pitch angle
C	=	chord length
C_d	=	drag coefficient
C_l	=	lift coefficient
C_P	=	power coefficient
i	=	current
K_v	=	motor speed constant
λ	=	tip speed ratio
λ_h	=	tip speed ratio, hub radius
λ_r	=	tip speed ratio, outer radius
M	=	molar mass

*Undergraduate, Department of Mechanical and Aerospace Engineering, AIAA Student Member 1603357
†Undergraduate, Department of Mechanical and Aerospace Engineering, AIAA Student Member 953530
‡Undergraduate, Department of Statistics, AIAA Student Member 1605501
§PhD, Department of Mechanical and Aerospace Engineering, AIAA Student Member 1605506

μ = dynamic viscosity of air
n = number of blades
ϕ = velocity direction
P = power
P_{wt} = pressure in the wind tunnel
R = radius of blade and hub
R_{air} = ideal gas constant
R_i = radial position of the element in relation to the center of the hub
R_L = Load Resistance
ρ = density
r = motor internal resistance
ψ = skew angle
τ_p = elemental pitch angle
T_{wt} = temperature
θ = turbine blade azimuth angle
V_∞ = free-stream velocity
v = applied voltage
Ω = rotation rate of the turbine

II. Introduction

Wind energy harvesting through specially designed turbines provides a renewable source of energy to power modern society. Advancement in the technology required to increase the efficiency of wind energy harvesting is vital to ensure that renewable energy investments maximize the productivity of future turbine units. Wind turbine efficiency is governed by Betz's law, published in 1919 by Albert Betz [1]. This law states that through the assumptions of a non-rotating wake, an infinite number of blades, steady-state rectilinear incompressible flow, and zero frictional drag, the maximum energy transformation from fluid flow to mechanical power is limited to an efficiency of 0.5926 [1]. Future innovations in turbine blade efficiency will increasingly attempt to approach this theoretical value with efficient airfoil selection, turbine blade twist optimization, and lightweight structural components [2]. To measure the efficiency of real-world turbine blades, a concept known as the power coefficient can be utilized. This fraction denotes the power generation measured by the wind turbine compared to the theoretical potential energy stored in the moving fluid [3].

$$C_P = \frac{P}{\frac{1}{2}\rho V_\infty^3 A} \tag{1}$$

Many of the simplification assumptions utilized in Betz turbine analysis such as a lack of tip vortex loss and 3D effects are contrary to the real-world mechanics involved in wind energy harvesting. A central deviation from this is the assumption of axial flow to the turbine. The theoretical maximum power generation occurs when the inflow velocity direction is aligned with the axis of rotation of the turbine, but this is often not the case with the variability in magnitude and direction of airflow moving through the control volume of a wind turbine. Within this analysis, inflow velocity that is not along the turbine axis of rotation will be denoted as the term "skewed" flow, which will be defined by a magnitude and skew angle. Some modern turbines are equipped with active or passive yaw systems in an attempt to minimize this skew angle during turbine operation, but these systems can be costly to implement and require a finite time to adjust the directionality of the turbine, leading to efficiency decreases from a theoretical maximum energy harvest [4].

In order to design turbine blades for maximum energy extraction, there are three main optimization characteristics. The first is chord optimization, which involves optimizing the Reynolds number towards a desired values across the span of the rotating blade [3]. The second is airfoil selection, which can be done through brute force selection or, more elegantly, with methods such as a genetic [5] or gradient descent [6] algorithms to decrease the computation cost associated with selection. The final parameter is the twist distribution across the blade span, which places each airfoil at its optimal angle of attack across the span of the blade, generating maximum aerodynamic forces when subject to inflow. Each of these parameters has well-defined optimization schemas for axial flow conditions; however, for the case of a skewed inflow, a novel optimization schema was developed.

III. Turbine Blade Modeling

A. Reynolds Number Characterization

To develop a blade optimization methodology, the discretization of a turbine blade into a finite number of elements must be completed. This concept, known as blade element momentum theory (BEMT) [7], allows for characteristic properties of the blade to be determined at defined intervals, and the integration of these properties reflects the total aerodynamic priorities of the continuous blade. A uniform elemental distribution was used in this analysis for computational simplicity. To begin the analysis, an axis definition diagram has been provided in Figure 1.

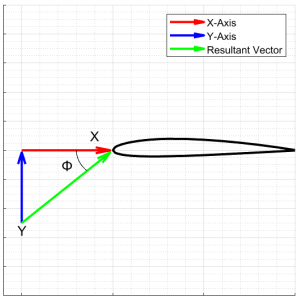

Fig. 1 Blade element axis definition diagram.

To determine the seen inflow velocity of each segment, the vector component analysis of the three main velocity components was performed free from the influence of wake induction factors. The inflow velocity components defined in relation to the blade axis and free-stream velocity are as follows.

$$V_{x,inflow} = V_{\infty} cos(\psi) \tag{2}$$

$$V_{y,inflow} = V_{\infty} sin(\psi) sin(\theta) \tag{3}$$

Where ψ represents the skew angle of the turbine, and θ represents the turbine blade azimuth angle across its rotational domain. The rotational velocity for steady state operational of the blade is given by:

$$V_{y,rotation} = \Omega R_i \tag{4}$$

Where Ω is the rotational rate of the turbine, and R_i is the elemental radius of the blade from the center point of the hub. To derive the influence of the skewed turbine's translational progression and regression with respect to the inflow velocity direction, the position and velocity function can be derived utilizing the chain rule with respect to the turbine azimuth angle θ across its domain.

$$x_{skew} = sin(\psi) R_i cos(\theta) cos(\psi) \tag{5}$$

$$V_{x,skew} = -\Omega sin(\psi) R_i sin(\theta) cos(\psi) \tag{6}$$

Within this formula, the cosine term represents the translation of the rotational velocity along the direction of incoming flow to the turbine axis, and the sine term represents the angular offset that creates this motion. Performing the vector magnitude formula yields the total seen velocity at each element of the turbine blade.

$$V_{seen} = \sqrt{(V_{x,inflow} + V_{x,skew})^2 + (V_{y,inflow} + V_{y,rotation})^2} \tag{7}$$

As expected, the velocity distribution is bimodal, with a larger amplitude for the section of azimuth where the skew velocity is aligned with the inflow direction and a shallower amplitude when the skew velocity opposes the inflow velocity. The seen velocity angle relative to the blade axis can be determined using the trigonometric relationship:

$$\phi_{seen} = tan^{-1}((V_{y,inflow} + V_{y,rotation})^2 / (V_{x,inflow} + V_{x,skew})^2) \tag{8}$$

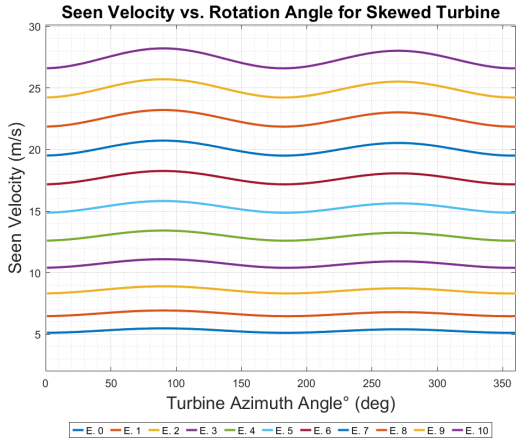

Fig. 2 Elemental seen velocity versus turbine azimuth angle for V_∞ = 5 m/s. λ = 5.23.

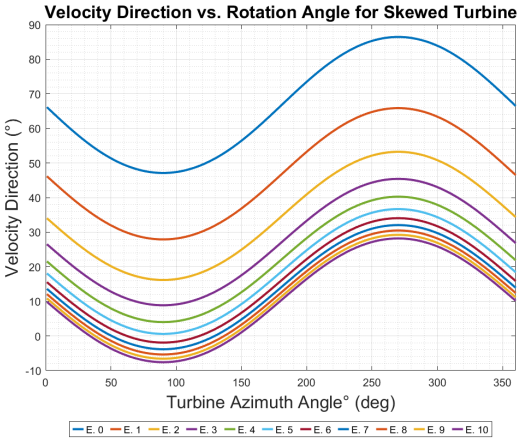

Fig. 3 Elemental seen velocity direction versus turbine azimuth angle for V_∞ = 5 m/s. λ = 5.23.

From Figure 3, the vertical shift due to the predominant inflow velocity magnitude of inner elements can be observed for the uniform pitch distribution in this example. The negative values for tip elements indicate that the skew velocity overcomes the inflow velocity to produce a total velocity opposite the airfoil's assigned coordinate system. To determine the elemental Reynolds number, the density of the inflow air can be derived using the ideal gas law for the assumed thermodynamic state of the wind tunnel.

$$\rho = \frac{P_{wt} M}{R_{air} T_{wt}} \tag{9}$$

Finally, the elemental chord length can be determined using a wake-rotation assumption for best practices with experimental conditions [3]. The average value of the seen velocity direction is used in equation 10

$$C = \frac{8\pi R_i}{nC_l}(1 - cos(\phi_{seen})) \tag{10}$$

The Reynolds number used for further analysis is then determined by taking the average value across the azimuth sweep of the turbine blade from equation 8.

$$Re = \frac{\rho V_{seen,avg} C}{\mu} \tag{11}$$

B. Airfoil Selection

To select efficient airfoils for use in turbine elemental definition points, the panel numerical method developed by Drela known as Xfoil was used[8].To reduce computational resources associated with airfoil selection, a genetic algorithm approach was utilized due to the unknown nature of the gradient outputs of airfoil selection, which may lead to a local maxima being selected as the best candidate airfoil.

The outline of this minimum genetic algorithm is such that an initial population of candidates is randomly selected from all possible NACA 4-series airfoils. The Xfoil command interface developed by Oliveira [9]can be used to generate lift and drag polar's across the attached flow sections of each airfoil using the average Reynolds number and mach number found in section A. To optimize turbine performance, the summation of lift over drag ratio across the regime can be stored and stored at the end of the process. Once each candidate has been characterized or abandoned due to lack of convergence at the specified Reynolds number, parent candidates can be selected based on the top-performing airfoils. These parent's airfoils generate offspring that average the characteristics of the best-performing airfoils until the number of offspring has been met. To prevent the highest-performing airfoils from being removed from the next generation due to inefficiency in the minimal algorithm, a specified set of highest-performing airfoils is manually established into the offspring generation. This process is then repeated for the specified number of generations until a single best-performing candidate is selected. It is important to note that the current version of this genetic algorithm does not support a methodology for offspring mutation due to the sophistication of the algorithm, but future work should include this functionality for better algorithm performance. A sample visualization of the airfoil selection across generations has been provided.

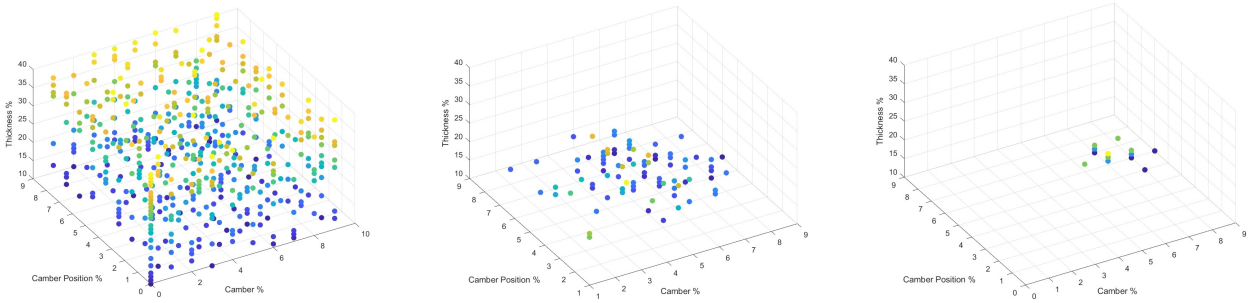

(a) Initial population. (b) Third generation. (c) Fifth generation

Fig. 4 Genetic algorithm selection of airfoil properties.

C. Twist Generation

To ensure each elemental airfoil is placed at the optimal pitch angle for maximum lift-over-drag performance, a twist distribution must be generated. For axial flow turbines, the velocity variation with azimuth angle remains constant; thus, the twist generation can easily be performed. Multiple methods have been proposed to arrive at the optimal twist distribution, with the most well-known introduced by Betz [1].

$$\beta = tan^{-1}(\frac{2}{3\lambda_r}) \tag{12}$$

For twist optimization for a skewed turbine, the approach was taken to analyze characteristics that maximize contributions to the power coefficient specifically [3]

$$C_P = \frac{8}{\lambda^2}\int_{\lambda_h}^{\lambda} \lambda^3 a'(1-a)[1-(\frac{C_d}{C_l})cot\phi]\, d\lambda_r \tag{13}$$

For use within the optimization, equation 13 can be expanded for a variable inflow direction across the azimuth domain of the turbine.

$$C_P = \frac{8}{\lambda^2}\int_{\lambda_h}^{\lambda}\int_{\theta_0}^{\theta} \lambda^3 a'(1-a)[1-(\frac{C_d(\alpha)}{C_l(\alpha)})cot(\phi(\theta))]\, d\lambda_r\, d\theta \tag{14}$$

Along with the required transformation function from Manwell [3].

$$\alpha(\theta) = \phi(\theta) - \tau_p \tag{15}$$

For optimization across the domain of elemental pitch angles, the Viterna method [10] of airfoil polar extrapolation beyond the bounds discussed in section B can be utilized.

$$C_l = A_1 sin^2\alpha + A_2 \frac{cos^2\alpha}{sin\alpha} \tag{16}$$

$$C_d = B_1 sin^2\alpha + B_2 cos\alpha \tag{17}$$

Where

$$C_{d_{max}} \approx 1.11 + 0.018AR \tag{18}$$

$$A_1 = \frac{C_{d_{max}}}{2} \tag{19}$$

$$B_1 = C_{d_{max}} \tag{20}$$

$$A_2 = (C_{l_{stall}} - C_{d_{max}} \sin\alpha_{stall} \cos\alpha_{stall}) \frac{sin\alpha_{stall}}{cos^2\alpha_{stall}} \tag{21}$$

$$B_2 = \frac{C_{d_{stall}} - C_{d_{max}} sin^2\alpha_{stall}}{cos\alpha_{stall}} \tag{22}$$

Utilization of equations 16 and 17 with the accompanying empirical factors with equation 14 allows for the optimal elemental pitch angle τ_p to be calculated by performing a pitch angle sweep and locating the maximum value for the inner integral. Special consideration must be made for airfoils that approach zero C_l within the pitch angle sweep and for ϕ values that cross the origin, both generating an asymptotic value that skews the optimization.

IV. Turbine Design

To validate the optimization schema introduced in section III, experimental turbine blades were developed using specific initial conditions. An inflow velocity of 5 meters per second and a skew angle of 30 and 20 degrees were selected. Previously manufactured turbine hubs contained slots for a 3-blade rotor. The blade was discretized into 10 elements to balance opportunities for optimization with computational resources. Thus, this constraint was necessitated. For airfoil selection, an optimal tip speed ratio was calculated using the following optimal tip speed ratio equation [11] yielding a tip speed ratio of 5.23.

$$\lambda_{opt} \approx \frac{4\pi}{n}(\frac{5}{4}) \tag{23}$$

Due to size constraints with the experimental setup, structural concerns arose with the use of specific chord distributions such as equation 10. As a result, a constant chord was used to allow for interior reinforcement of the blade through the use of a spar. Reynolds number and velocity direction characterization resulted in Figures 2 and 3, respectively. Utilization of the genetic algorithm for airfoil selection with a parent population consisting of 50% of the NACA 4-series domain. Five generations were run with a decrementing residual population. The resulting airfoils have been tabulated.

Table 1 NACA 4-series genetic algorithm results for 20° skew and 30° skew.

Element Number	0	1	2	3	4	5	6	7	8	9	10
20° Skew	9710	6710	6710	7710	7810	5510	4510	5510	5510	6510	5510
30° Skew	7710	5710	6710	7710	6710	6710	4510	5510	5510	6510	5510

The Betz twist optimization was then conducted for the base blade, and initial simulations were conducted within the QBlade [12] to estimate the axial induction factor a and the tangential induction factor a-prime. Higher fidelity simulations of these values across the azimuth sweep provide better estimates than hand calculation. A sample output of the twist optimization function discussed in section III.C has been provided in Figure 5.

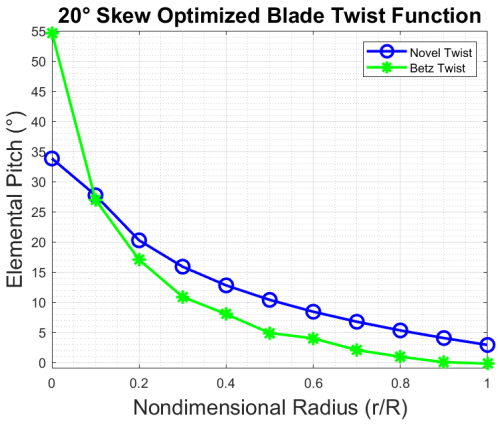

(a) Twisting function for 20 degrees of skew.

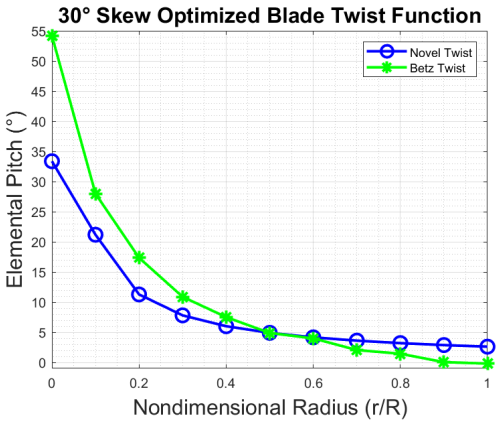

(b) Twisting function for 30 degrees of skew.

Fig. 5 Twisting function distribution comparison.

It is observed in Figure 5 that greater amounts of skew yield a higher slope decent across the blade element sweep, with the root pitch most influenced by the novel twist methodology. The point of intersection between the two curves is also shifted right as the skew angle increases.

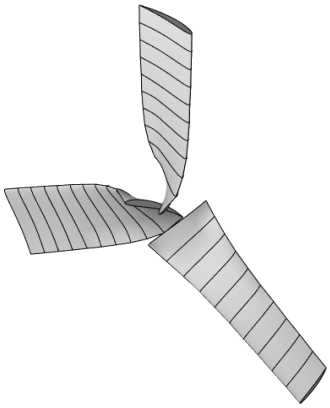

(a) Betz optimized blades.

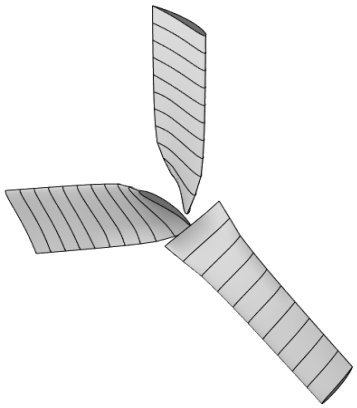

(b) Novel optimized blades.

Fig. 6 Geometry comparison for blades optimized for 30 degrees of skew.

To generate theoretical results for blade performance, free vortex BEMT can be used within Qblade shown in Figure 7a. The results of the simulation are shown in Figure 7b with the novel turbine generates a higher peak power at all skew conditions, ranging from 14.6% at 20° skew and 19.7% at 0° skew.

V. Experimental Design

To test the methodology, a subsonic wind tunnel testing environment was utilized. The subsonic wind tunnel at NC State has capabilities to support changes in pitch and yaw, while mounting an assembly to a sting to negate mounting

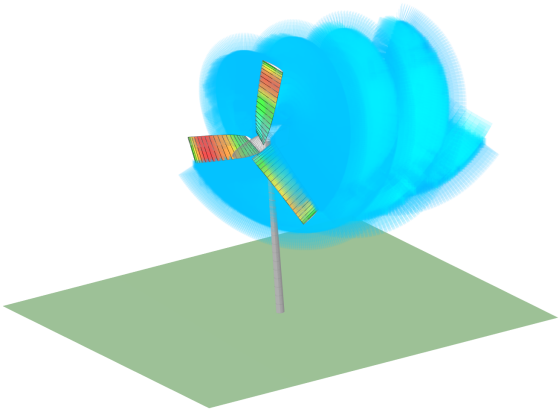

(a) Free Vortex BEMT Simulation in QBlade.

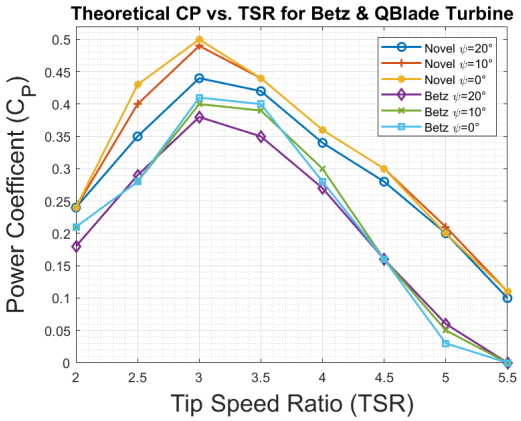

(b) Theoretical power coefficient comparison.

Fig. 7 Theoretical C_P plot generation and comparison.

effects. The design process for this experimental assembly prioritized robustness and modular design, allowing for efficient blade changes during testing.

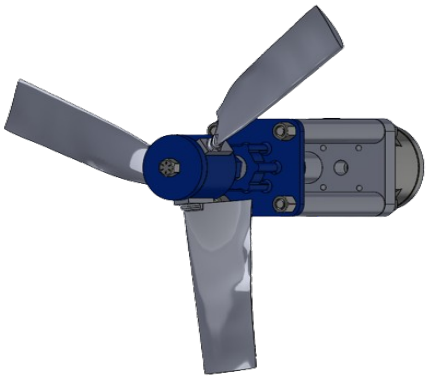

(a) Turbine characterization experimental setup.

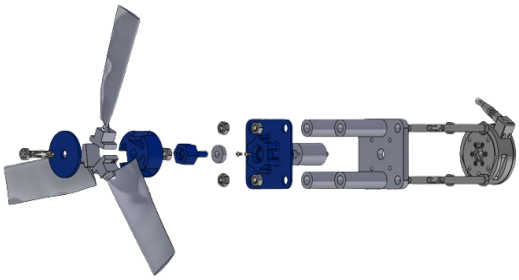

(b) Experimental setup exploded view.

Fig. 8 Experimental setup.

The experimental design is divided into three sub-assemblies shown in Figure 8. Firstly, the mounting sub-assembly is utilized to securely and rigidly connect the sting to the assembly. Several mounting plates connect the assembly to the sting, and rigidly secures the ATI Force/Torque load cell to the rest of the assembly. Secondly, the motor-mounting assembly includes support infrastructure for the motor during operation and allows for quick replacement of parts in the case of failure. Lastly, the blade mounting sub-assembly is made so that blades can be easily and quickly changed between experiments to increase efficiency during testing.

During the early stages of the design phase, some simple calculations were completed to analyze the effectiveness of different DC motors as generators in the approximate experimental conditions. Utilizing these results, a motor was selected due to its ability to adequately handle the expected high rotation rate of the blades, power output, and current based on its motor characteristics.

The radius of the blade and hub assembly was chosen to be 0.15 meters so that the wall effects of the wind tunnel would not impact the experimental results. The blades were designed according to the genetic algorithm, however, it was noticed that the genetic algorithm selected thin blades to maximize power. Due to the short length of the blades and small chord length and thickness at the tip, the first design of the blade was not able to be fabricated without compromising structural strength. Thus, to ensure structural integrity of the blades during operation, the genetic algorithm was utilized such that the expected output airfoils were no less than 5 millimeters thick, as shown in Figure 9. A 2.38 millimeter

steel spar was also utilized to strengthen the blades during operation at high rotation rates.

(a) With taper. (b) Constant chord.

Fig. 9 Blades optimized for 30 degrees of skew.

Many of the custom parts used in the assembly were 3D printed using ABS filament, including the blades, the motor mounting plate, and the blade hub. The final assembly was mounted in the wind tunnel, see Figure 10.

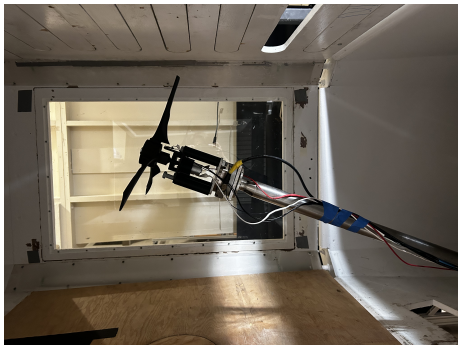

Fig. 10 Experimental setup within the wind tunnel test section.

In the experiment, an ATI Force/Torque Gamma load cell was used to record force and torque values in all three directions. A Hall effect sensor was used to measure the rotation of the blades, using small neodymium magnets that were installed on the blade hubs. To record the output data from the load cell and hall effect sensor, a PXE data acquisition system was utilized using a LabVIEW program that was designed for this experiment. A ET540 electronic programmable load was also utilized to vary the resistance applied to the system, so that the rotation rate could be controlled and various C_P at different tip speed ratios. Lastly, the motor generated both current, voltage, and derived wattage which were measured and recorded using an oscilloscope. Due to the mechanical skew limitations of the wind tunnel's sting mount, only the 20° optimized blades were manufactured for this experiment. Each blade was optimized for 20 degrees of skew, with one blade being optimized using Betz twist optimization, and the other being optimized using this methodology.

VI. Experimental Results

During the experiment, the blades optimized for 20 degrees of skew using the Betz and novel approach were each tested at 0, 10, and 20 degrees of skew. For the tests at 20 degrees of skew, 18 different loading conditions were tested with resistance values between 100 and .03 ohms. The tests at 0 and 10 degrees of skew were tested with 11 different loading conditions with resistance values between 50 and 0.03 ohms. To observe the performance of different blades, a Python script was written and utilized to plot C_P versus tip speed ratio (λ) for each blade. To perform this transformation, the rotational speed cataloged using the Hall effect sensor was divided by the wind tunnel flow speed

setting according to equation 24. The power generation from the turbine was found by utilizing the oscilloscope over the motor to record a voltage measurement across a steady state sample, and divided by the resistance applied by the ET540 electronic programmable load according to equation 25. The resultant power was then divided by the available power to determine the power coefficient according to equation 1 and the resulting output is seen in Figure 11.

$$TSR = \frac{\Omega R}{v_\infty} \tag{24}$$

$$P = \frac{v^2}{R_L} \tag{25}$$

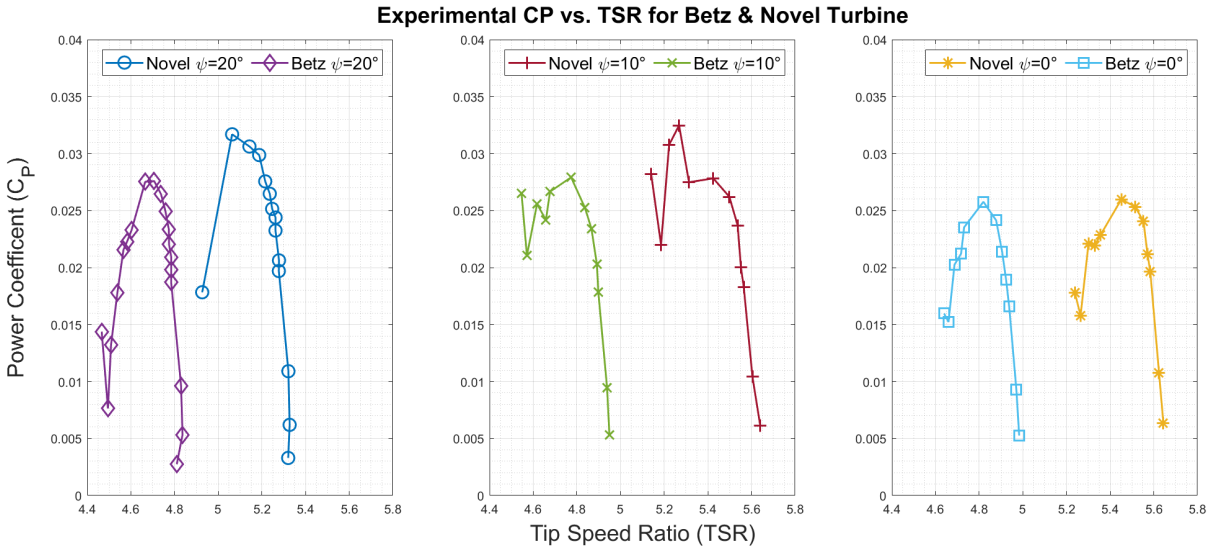

Fig. 11 Experimental results of the novel and Betz blade characterization.

In the experiment, it was observed that the novel optimized blade generated higher maximum power coefficient values than the Betz optimized blade at 20° and 10° of skew and mirrored the power coefficient performance in the 0° skew condition. However, the motor selected was only able to provide a small amount of braking to the turbine system, which prevented a larger range of tip speed ratios from being observed. Each of the skew angles demonstrate a higher tip speed ratio indicating better airfoil performance compared to the Betz optimized blade.

Conclusion

The purpose of this study was to demonstrate a novel methodology for both airfoil selection via genetic algorithm and twist optimization for a wind turbine in skewed fluid flow. Through both theoretical and experimental work, it was observed that the optimized blade was providing higher power coefficients and an increase in tip speed ratio in optimal skew conditions, but the motor was not able to provide enough braking for a wider range of tip speed ratios to be observed. To further analyze the success of these methodologies, more research into the theory behind this methodology must be conducted, and more experimental validations using better motors must also be carried out.

Acknowledgements

The authors would like to thank Dr. Andre Mazzoleni and the members of the NCSU Engineering Mechanics and Space Systems Laboratory for their support of the project. The authors would also like to thank Dr. Mingtai Chen for support with the wind tunnel experimental setup.

References

[1] Betz, A., *Introduction to the Theory of Flow Machines*, 1st ed., Pergamon Press, 1966.

[2] Metoyer, R. M., "Modeling, Simulation, and Analysis of Tethered Horizontal Axis Fluid Energy Conversion Systems," *Energy Conversion and Management*, Vol. 243, 2021. https://doi.org/https://doi.org/10.1016/j.enconman.2021.113929.

[3] Manwell, J. F., McGowan, J. G., and Rogers, A. L., *Wind Energy Explained: Theory, Design and Application*, John Wiley & Sons, Chichester, UK, 2002.

[4] Yang, J., Fang, L., Song, D., Su, M., Yang, Z., Huang, L., and Joo, Y. H., "Review of Control Strategy of Large Horizontal-Axis Wind Turbines Yaw System," *Wind Energy*, Vol. 24, 2020, pp. 97–115.

[5] Antunes, A. P., Azevedo, L. L. F., and de Castro Santos, L. C., "Airfoil Shape Optimization Using Genetic Algorithms," *International Congress of Mechanical Engineering*, 2003.

[6] Mirzaei, M., Roshanian, J., and Hosseini, S. N., "Aerodynamic Optimization of an Airfoil Using Gradient Based Method," 2006.

[7] Moriarty, P. J., and Hansen, A. C., *Aerodyn Theory Manual*, U.S. Department of Energy, 2005. URL https://www.nrel.gov/docs/fy05osti/36881.pdf.

[8] Drela, M., "XFOIL Subsonic Airfoil Development System," MIT, n.d. URL https://web.mit.edu/drela/Public/web/xfoil/, accessed: [Insert access date here].

[9] Oliveira, R., "Rafael-Aero/xfoilinterface," MathWorks File Exchange, 2016. URL https://www.mathworks.com/matlabcentral/fileexchange/30478-rafael-aero-xfoilinterface.

[10] Mahmuddin, F., Klara, S., Sitepu, H., and Hariyanto, S., "Airfoil Lift and Drag Extrapolation with Viterna and Montgomerie Methods," *Energy Procedia*, Vol. 105, 2017, pp. 811–816. https://doi.org/https://doi.org/10.1016/j.egypro.2017.03.394, 8th International Conference on Applied Energy, ICAE2016, 8-11 October 2016, Beijing, China.

[11] Ragheb, M., and Ragheb, A. M., "Wind Turbines Theory - The Betz Equation and Optimal Rotor Tip Speed Ratio," InTechOpen, 2010. https://doi.org/https://doi.org/10.5772/21398.

[12] QBlade.org, "QBlade - Next Generation Wind Turbine Simulation," https://qblade.org/, 2023. Accessed: 2023-09-18.